Discrimination of yellowfin tuna Thunnus albacares between nursery areas in the Indian Ocean using otolith chemistry

Iraide Artetxe-Arrate, Igaratza Fraile, Naomi Clear, Audrey M. Darnaude, David L. Dettman, Christophe Pécheyran, Jessica Farley, Hilario Murua

Vol. 673: 165–181, 2021
https://doi.org/10.3354/meps13769

MARINE ECOLOGY PROGRESS SERIES
Mar Ecol Prog Ser

Published September 2

Discrimination of yellowfin tuna *Thunnus albacares* between nursery areas in the Indian Ocean using otolith chemistry

Iraide Artetxe-Arrate[1,*], Igaratza Fraile[1], Naomi Clear[2], Audrey M. Darnaude[3], David L. Dettman[4], Christophe Pécheyran[5], Jessica Farley[2], Hilario Murua[6]

[1]AZTI, Marine Research, Basque Research and Technology Alliance (BRTA), Pasaia, Gipuzkoa 20110, Spain
[2]CSIRO Oceans and Atmosphere, Hobart, Tasmania 7000, Australia
[3]Marbec, Univ Montpellier, CNRS, Ifremer, IRD, 34095 Montpellier, France
[4]Environmental Isotope Laboratory, Department of Geosciences, University of Arizona, Tucson, AZ 85721, USA
[5]IPREM, Institut des sciences analytiques et de physico-chimie pour l'environnement et les matériaux, Université de Pau et des Pays de l'Adour, 64000 Pau, France
[6]International Seafood Sustainability Foundation, Washington, DC 20005, USA

ABSTRACT: Yellowfin tuna *Thunnus albacares* is a highly exploited species in the Indian Ocean. Yet, its stock structure is still not well understood, hindering assessment of the stock at a suitable spatial scale for management. Here, young-of-the-year (<4 mo) yellowfin tuna otoliths were collected in 2018 and 2019, from 4 major nursery areas in the Indian Ocean: Madagascar, Seychelles-Somalia, Maldives and Sumatra. First, direct age estimates were made in a subset of otoliths by visually counting microincrements to identify the portion of the otolith corresponding to the larval stage. We then developed 2-dimensional maps of trace element concentrations to examine spatial distribution of elements across otolith transverse sections. Different distribution patterns were observed among the elements analysed; Li, Sr and Ba were enriched in the portion of the otolith representing early life, whereas Mn and Mg concentrations were heterogeneous across growth bands. Last, we analysed inter-annual and regional variation in otolith chemical composition using both trace elements (Li, Mg, Sr, Ba and Mn) and stable isotopes ($\delta^{13}C$ and $\delta^{18}O$). Significant regional variation in otolith chemical signatures was detected among nurseries, except between Madagascar and Seychelles-Somalia. Otolith $\delta^{13}C$ and $\delta^{18}O$ were important drivers of differentiation between western (Madagascar and Seychelles-Somalia), Maldives and Sumatra nurseries, whereas the elemental signatures were cohort specific. Overall nursery assignment accuracies were 69–71%. The present study demonstrates that baseline chemical signatures in the otoliths of yellowfin tuna are regionally distinct and can be used as a natural tag to investigate the nursery origin of older individuals in the Indian Ocean.

KEY WORDS: Otolith microchemistry · Yellowfin tuna · Otolith elemental fingerprints · Nursery discrimination · Trace elements · Stable carbon and oxygen isotopes · Stock structure

1. INTRODUCTION

Yellowfin tuna *Thunnus albacares* is an important source of food, employment and livelihood for numerous nations, and an important commercial species in the global fisheries market (FAO 2016, Guillotreau et al. 2017). As such, this species experiences significant fishing pressure, with global catches reaching about 1.45 Mt in 2018 (FAO 2020). Of the 4 yellowfin tuna stocks managed in world oceans, the Indian

*Corresponding author: iraide.artetxe@azti.es, i.artetxe73@gmail.com

Ocean stock is currently considered overfished and subject to overfishing (IOTC 2020, ISSF 2020). The Indian Ocean Tuna Commission (IOTC) assessment assumes that yellowfin tuna constitutes a single stock in the Indian Ocean owing to the rapid and large-scale movements observed in the Indian Ocean Regional Tuna Tagging Program (IOTC 2021). However, the single-stock paradigm has been questioned, as findings derived from regional genetic and parasite studies suggested a more fragmented structure than the one currently considered for the assessment of this species (Dammannagoda et al. 2008, Kunal et al. 2013, Moore et al. 2019).

Although adult yellowfin tuna are distributed across the entire Indian Ocean as far south as 45° S (Sharp 2001), their spawning activity is restricted to particular environments with warmer temperatures and with mesoscale oceanographic activity, such as fronts or eddies (Schaefer 2001, Reglero et al. 2014, Muhling et al. 2017). Bottom topography is also an important factor determining spawning grounds, with greater abundance of larvae near land masses, particularly islands, compared to offshore waters (Boehlert & Mundy 1994). Early surveys of larvae confirmed a patchy larval distribution of yellowfin tuna along the Indian Ocean (Ueyanagi 1969, Conand & Richards 1982, Nishikawa et al. 1985). The main spawning grounds of yellowfin tuna in the Indian Ocean are located in the equatorial (0–10° S) area and west of 75° E (IOTC 2021). Spawning has been documented for yellowfin tuna in waters around the Seychelles, off Somalia and off Madagascar in the western Indian Ocean (Zudaire et al. 2013), the Maldives and Chagos Archipelagos in the west-central Indian Ocean (Zhu et al. 2008) and off Sri Lanka and west of Sumatra in the northeastern Indian Ocean (Nootmorn et al. 2005).

However, the relative importance of different spawning and nursery areas to the total catches and the degree of connectivity and mixing rates of yellowfin tuna in the Indian Ocean are still unknown. Ignoring complex stock structure and connectivity can lead to a misperception of fish productivity and wrong predictions of future stock abundance (Kerr et al. 2017). When the stock structure is more complex than recognized, local overexploitation and possible collapse of less productive stocks may occur and, hence, ignoring the stock structure of a species can lead to a suboptimal utilization of the resource (Ying et al. 2011). Therefore, the understanding of the stock structure of any species, and particularly of highly exploited species such as yellowfin tuna, is essential to develop a suitable spatial scale for management (Kerr et al. 2017, Bosley et al. 2019).

The chemical composition of fish otoliths (i.e. earbones) can be an effective tool to identify nursery areas and thus provide information on stock structure, which is important for determining the appropriate spatial scale at which a species should be managed (Campana 1999, Kerr et al. 2020). This technique has proved to be useful to study the origin and connectivity of yellowfin tuna in other oceans (Wells et al. 2012, Rooker et al. 2016, Kitchens et al. 2018). Otoliths are composed of a calcium carbonate ($CaCO_3$) structure in the form of aragonite (98%), on a non-collagenous organic matrix (2%) (Campana 1999). Otoliths are acellular and metabolically inert and, as such, material accreted during otolith formation is preserved as a fish grows (Campana & Neilson 1985). Counts of daily increments in otoliths can be used to select the portion of the otolith to be assayed that corresponds to the age of interest, such as the larval phase of the fish (Campana & Thorrold 2001). During the biomineralization process, chemical elements are incorporated into the otolith at minor and major concentrations, by either direct Ca substitution, random trapping in the interstitial spaces of the crystal lattice or interaction with otolith proteins (Campana 1999, Izzo et al. 2016, Thomas et al. 2017). Most otolith chemistry studies have focussed on elements that are dominant in the salt fraction of the otolith (e.g. Li, Mg, Sr, Ba, Mn, $\delta^{13}C$ and $\delta^{18}O$), while other elements strongly associated with the proteinaceous fraction (e.g. Zn and Cu) have also been used in trace element fingerprinting (Thorrold et al. 1997, Thomas et al. 2020). The uptake of the elements is regulated by a range of intrinsic and extrinsic factors, and thus the otolith chemical composition reflects a combination of physico-chemical factors of the environment inhabited by the fish, and other intrinsic factors such as physiology, diet, ontogeny and genetics (Hüssy et al. 2020, Macdonald et al. 2020). The chemical composition of the otolith material accreted during early life stages, therefore, serves as a 'chemical fingerprint' that may differ among groups of fish belonging to different nursery areas (Campana 1999).

We aimed to determine whether young-of-the-year (YOY) yellowfin tuna from different nursery areas in the Indian Ocean have distinct chemical signatures in their otoliths. If so, the chemical signatures can be used to develop baseline signatures that allow us to retrace the origin of older fish and determine the contribution of these nurseries to the different yellowfin tuna spawning and feeding zones. A better understanding on the connectivity and mixing rates will help to inform fishery managers on yellowfin stock structure in the Indian Ocean and to determine

whether the species should be managed as several discrete stocks. A combination of trace elements and carbon and oxygen stable isotopes ($\delta^{13}C$ and $\delta^{18}O$) in otoliths of YOY yellowfin tuna captured in 4 nursery regions were analysed. Specifically, we (1) estimated age at early life to assist the interpretation of otolith microchemistry, (2) analysed the distribution of trace elements throughout the otolith to better understand elemental uptake variability within the otolith and (3) assessed the temporal and spatial variation of the chemical signatures both within and between individuals caught in different nursery areas and on different collection dates.

2. MATERIALS AND METHODS

2.1. Sample collection

Samples were obtained by scientific observers on-board purse seine vessels or in port landings, as part of a collaborative research project on the population structure of tuna, billfish and sharks of the Indian Ocean (Davies et al. 2020). A standard operating procedure was followed to ensure a standardized sample collection. Capture location was available with a maximum of 5° × 5° quadrant range, and sampling of fish belonging to the same school was limited to 5 individuals. YOY yellowfin tuna (n = 113) were collected from 4 geographically distinct nursery areas in the Indian Ocean: Madagascar, Seychelles-Somalia, Maldives and Sumatra (Fig. 1). In this study, we define nursery areas as primary regions inhabited by YOY yellowfin tuna in the Indian Ocean, which are therefore considered as important habitat during the first year of life (Wells et al. 2012). Sampling was conducted over short periods during 2 consecutive years, 2018 and 2019 (Table 1). Fish were measured (fork length [FL] to the nearest centimetre), and sagittal otoliths were extracted with stainless steel tweezers,

Table 1. Summary of young-of-the-year yellowfin tuna *Thunnus albacares* collected from 4 nursery regions of the Indian Ocean: Madagascar, Seychelles-Somalia, Maldives and Sumatra. Size is fork length (FL) in cm. Cohort was back-calculated using the age–length curve (Fig. 3) calculated in Section 2.2. No samples were available for the 2018 Madagascar cohort

Region	Cohort	Sampling period	n	FL range	Mean FL (SD)
Madagascar	2017	March 2018	19	26.0–37.5	30.6 (3.2)
Seychelles-Somalia	2017	March–April 2018	18	29.0–37.0	33.2 (2.2)
	2018	March–April 2019	14	28.0–34.0	30.4 (1.8)
Maldives	2017	August 2018	15	33.0–36.0	34.8 (0.9)
	2018	February 2019	16	28.0–33.0	30.9 (1.5)
Sumatra	2017	April 2018	16	19.5–33.0	27.0 (3.6)
	2018	November 2018	15	25.5–34.0	30.6 (2.9)

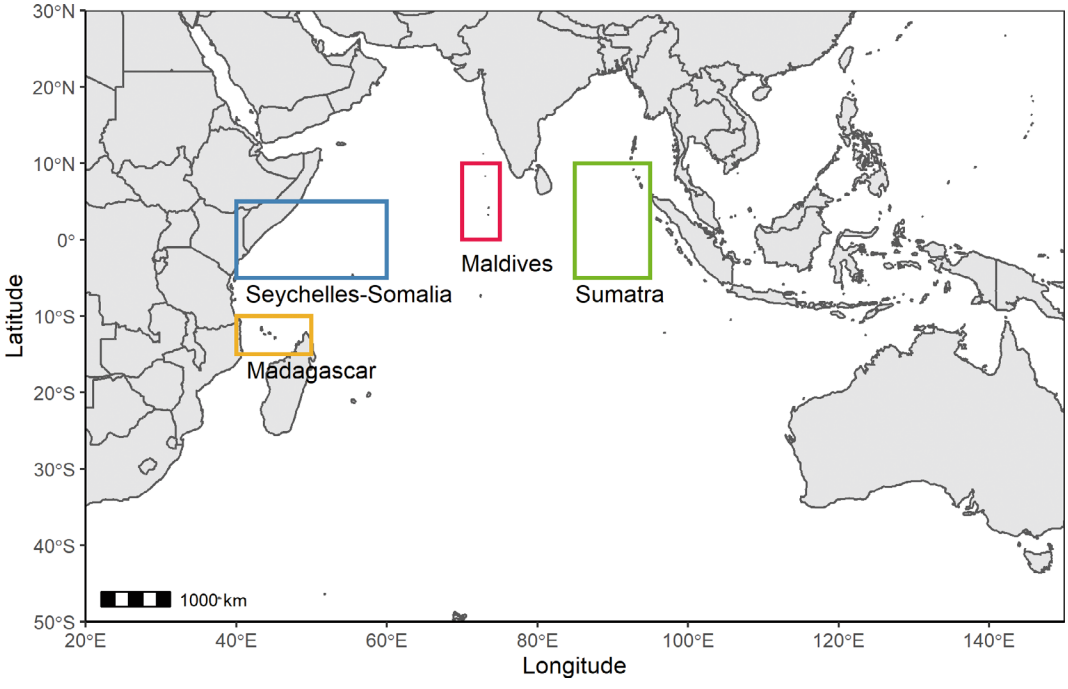

Fig. 1. Location of the 4 nursery areas for young-of-the-year yellowfin tuna *Thunnus albacares* in the Indian Ocean: Madagascar (yellow), Seychelles-Somalia (blue), Maldives (red), Sumatra (green)

cleaned of adhering organic tissue, rinsed with ultrapure water (Milli-Q) and stored dry in plastic vials (see Fig. S1 in the Supplement at www.int-res.com/articles/suppl/m673p165_supp.pdf). An effort was made to limit the size range (<38 cm FL), to ensure that the fingerprint of the YOY tuna reflected the chemical signature of the nursery ground where a fish was captured. The rationale for the latter is that YOY are characterised by a limited swimming ability and are not likely to have moved far from their larval nursery grounds (Kitchens et al. 2018, Pecoraro et al. 2018).

2.2. YOY age estimates

To be able to estimate the approximate age of the fish examined with otolith microchemistry, an age–length relationship curve was developed. For that, otolith sections (n = 5, from the Western Indian Ocean) were prepared following a 4-step process described by Proctor et al. (2019): (1) otoliths were fixed on the narrower edge of a crystal slide using thermoplastic glue (Crystalbond 509, Buehler) with the anterior side of the otolith hanging over the edge (with the primordium just on the inside of the glass edge), (2) the otolith was then ground down to the edge using 1200 and 600 grit sandpaper moistened with distilled water, and, when the edge of the slide was reached, (3) the slide was reheated and the otolith was removed and placed (ground side down) on another slide using thermoplastic glue. (4) Once cooled, the otolith section was ground horizontally to the grinding surface until the primordium was exposed, using a series of 3M® silicon carbide lapping discs (9, 3 and 1 µm) moistened with ultrapure water on a lapping wheel, and were further polished with a micro cloth and 0.3 µm aluminium powder to ensure a smooth surface.

Age interpretation was based on digital photographs taken under a transmitted light microscope at different magnifications (10, 20 and 40×). Images were analysed using the GNU Image Manipulation Program (GIMP) version 2.10.12. Age was determined by visually counting microincrements along the ventral (longer) arm of the section on a path from the primordium to the edge margin (Fig. S2). These counts were combined with direct increment counts on otoliths from Proctor et al. (2019) (n = 9, from the Eastern Indian Ocean), and *in situ* development observations from Kobayashi et al. (2015) (n = 3, tank reared) (Table S1). In addition, the count (age in days) was noted at 2 other points along the counting path of the 5 otoliths directly examined: at 65 µm from the primordium towards the ventral arm of the otolith, and at the first inflection point of the growth axis, where the direction of growth changes (Fig. S2).

2.3. Otolith preparation for microchemical analyses

When both otoliths were available, one was used for trace element analyses and the second for $\delta^{13}C$ and $\delta^{18}O$ analyses. When a single otolith was available, all chemical analyses were sequentially conducted on the same otolith. Otoliths from each fish were embedded in 2-part epoxy resin (Araldite 2020, Huntsman Advanced Materials). Resin blocks were polished using 3M® silicon carbide sandpaper (particle size = 220 µm) and a lapping wheel with a series of decreasing grain diameter (30, 15, 9, 3 and 1 µm) 3M® silicon carbide lapping discs, moistened with ultrapure water, to obtain a transverse section where the primordium was exposed. Sections were ultrasonically cleaned using ultrapure water for 10 min. Following sonication, otolith sections were left to air dry in loosely capped vials for 24 h before being glued in a sample plate using Crystalbond thermoplastic glue (Crystalbond 509, Buehler).

2.4. Multi-elemental 2D imaging

Otoliths of 3 individuals were selected to perform 2-dimensional mapping of multiple elements. These fish were collected in the Seychelles-Somalia, Maldives and Sumatra nurseries, during May, August and April 2018, and were 37, 35 and 32 cm FL, respectively. Elemental concentration was measured using a high-resolution inductively coupled plasma mass spectrometer (HR-ICPMS) fitted with a jet interface using an N_2 flow rate of 10 ml min^{-1} (Element XR, Thermo Scientific), coupled to a high repetition rate 1030 nm femtosecond laser ablation (fs-LA) system (Alfamet, Neseya, Canejan) available at the Institut des Sciences Analytiques et de Physico-Chimie pour l'Environnement et les Matériaux, Université de Pau et des Pays de l'Adour/CNRS (Pau, France). Imaging by fs-LA-HR-ICPMS was performed to analyse the elemental distribution of ^{7}Li, ^{24}Mg, ^{88}Sr, ^{138}Ba ^{55}Mn, ^{63}Cu, ^{66}Zn to Ca ratios along the ventral arm of otolith transverse sections, which represents the growth axis of the fish (Fig. 2A). The laser was operated at a repetition rate of 200 Hz, energy of 30 µJ per pulse and a beam size of 15 µm.

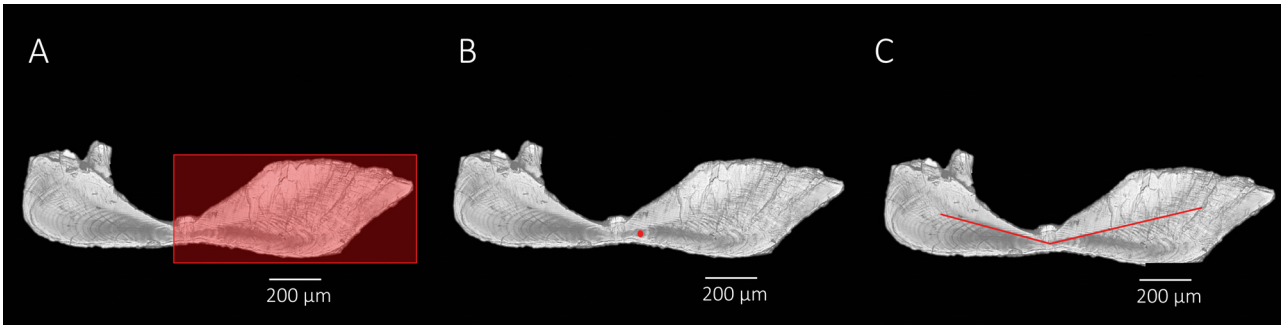

Fig. 2. Sagittal otolith transverse section from a young-of-the-year yellowfin tuna *Thunnus albacares* showing (A) the portion used for 2D chemical mapping (red box), (B) the approximate location of the laser ablation spot for trace element analyses (red dot) and (C) the MicroMill drilling path used for stable isotope analyses (red line)

The scanner was used in a fast and continuous back and forth movement of 15 µm at a speed of 1 mm s^{-1} to simulate an elongated laser beam (15 × 30 µm). Images were built from the fs-LA-HR-ICPMS signal resulting from the sample ablation according to a series of horizontal lines vertically distributed with 30 µm spacing (centre to centre). Considering that the washout time of the laser cell (based on the 99% criterion) was about 1 s and the ICPMS was set to acquire 0.67 points s^{-1}, the sample translation was set to 20 µm s^{-1}. This resulted in image resolution of 30 µm (square pixels of 30 µm). In these conditions, the signal corresponding to an image of 2.4 × 1.4 mm was acquired in 96 min. Data reduction and standardization to calcium (element:Ca µmol mol^{-1}) was done using the in-lab developed software FOCAL 2.27. The image matrix was then exported to the free ImageJ software (https://imagej.nih.gov/ij/) for better visualization and colour processing.

2.5. Trace element analysis

Otoliths were analysed for early life trace element composition with an fs-LA-HR-ICPMS. Laser ablation conditions were 200 Hz, a laser beam diameter of 15 µm and 30 µJ per pulse energy corresponding to a fluence of 14 J cm^{-2}, until the depth limit of ablation (<30 µm). The laser was fitted with a 2D galvanometric scanning beam device, allowing the fast movements of the laser beam (up to 500 µm s^{-1}) ablating the surface of the sample in a series of 6 concentric circle trajectories (Claverie et al. 2009). This resulted in the ablation of a crater 30 µm in diameter and 30 µm deep. This spot was ablated 65 µm from the primordium along the ventral arm (Fig. 2B), covering a signal of approximately 2–3 d according to Proctor et al. (2019). This spot was considered to be representative of the larval phase (see Section 3) and excluded the potential maternal effects the primordium may incorporate (Hegg et al. 2019). The ablation cell was flushed with argon to transport laser-induced particles to the HR-ICPMS. The fs-LA-HR-ICPMS was tuned daily to reach optimal particle atomization conditions and minimal elemental fractionation. This was obtained for a U:Th signal ratio of 1 ± 0.05 using the National Institute Standards and Technology (NIST) 612 glass standard. The mass spectrometer was used in the medium-resolution mode (R = 4000) to ensure a complete polyatomic interference removal for the isotopes of interest. Relative abundances of 7 isotopes (^{7}Li, ^{24}Mg, ^{88}Sr, ^{138}Ba ^{55}Mn, ^{63}Cu, ^{66}Zn) were estimated, as well as ^{43}Ca, which was used as the internal standard. The concentration of ^{43}Ca in the otolith was assumed to be constant at 38.3% (Sturgeon et al. 2005). Data reduction including background subtraction, conversion to ppm and standardization to Ca (element:Ca µmol mol^{-1}) was done using FOCAL 2.27. NIST 610 and 612 glass standards with known chemical composition were used for calibration. Measurement precisions were determined based on an otolith certified reference material for trace elements (FEBS-1, National Research Council Canada). To correct for short-term instrumental drift, standards and reference material were measured 3 times at the beginning, the middle and the end of each session (i.e. every 3–5 h). Trace element measurements of the blank sample gases were recorded for 20–30 s before each sample ablation of ~40 s. Mean relative standard deviation for NIST 612 and 610 were (n = 10): 5.8 and 4.6% (Li), 4.7 and 7.1% (Mg), 4.3 and 2.8% (Sr), 2.6 and 4.1% (Ba), 2.8 and 2.3% (Mn), 6.5 and 4.5% (Cu) and 6.8 and 4.16% (Zn), respectively. All elemental ratios exceeded the detection limits of the fs-LA-HR-ICPMS for all samples.

2.6. Stable isotope analysis

Microsampling of otolith powder $\delta^{13}C$ and $\delta^{18}O$ stable isotope analysis was performed using a high-resolution computerised micromill (New Wave Micro-Mill System, NewWave Research). The length of the smallest yellowfin tuna (19.5 cm FL) otolith section was used to create a template that was then used for the remaining otoliths to ensure that the same portion of the otolith was analysed in every fish. This drill path covered an area of the otolith that was estimated to represent the material accreted during the first ~2 mo of life, based on direct age estimates (Fig. 2C). A larger time period of the otolith was sampled for stable isotopes than for trace elements due to differences in sample material requirements. Ten drill passes were run at a depth of 50 µm per pass over a preprogramed drill path using a 300 µm diameter carbide bit (Komet dental, Gebr. Basseler). Powdered material was then analysed for $\delta^{13}C$ and $\delta^{18}O$ on an automated carbonate preparation device (KIEL-III, Thermo- Fisher Scientific) coupled to a gas-ratio mass spectrometer (Finnigan MAT 252, ThermoFisher Scientific) at the Environmental Isotope Laboratory of the University of Arizona. All isotope values are reported according to standards of the International Atomic Energy Agency in Vienna. The isotope ratio measurement was calibrated based on repeated measurements of NBS-19 and NBS-18 (International Atomic Energy Agency standards). Measurement precision was ±0.08‰ for $\delta^{13}C$ and ±0.10‰ for $\delta^{18}O$ (1 sigma).

2.7. Statistical analysis

All statistical analyses were performed using open access R software version 3.6.1 (R Core Team 2019). Prior to all multivariate analyses, otolith microchemistry data were scaled (i.e. for each element, the data were centred by subtracting the mean and scaled by dividing by the SD) to give the same weight to all elements and stable isotopes.

Normality and homoscedasticity of the data were tested using Shapiro-Wilks and Fligner-Killen tests, respectively. Not all elements and stable isotopes met the parametric assumptions (Tables S2 & S3). Consequently, to enable the combination of all elements for multivariate analyses, non-parametric tests were used. Interaction effects between nurseries and years in otolith microchemistry data were analysed using a 2-factor permutational multivariate analysis of variance (PERMANOVA) design for each element/isotope individually and all elements combined using the function 'adonis' in the R package 'vegan' (Anderson 2001, Oksanen et al. 2017). Nursery and cohort were fixed factors in the full factorial model, and resemblance matrix was based on Euclidean distance dissimilarities. The number of unrestricted permutations was set to 999 random repeats. Statistical significance was determined based on adjusted p-values after the Benjamini-Hochberg correction (Benjamini & Hochberg 1995). When significant differences were found, post hoc pairwise comparisons were applied to identify the source of differences between nursery means using the 'pairwise.adonis' function in 'pairwiseAdonis' (Martinez Arbizu 2020) in the case of multivariate data, and the 'lincon' function ('WRS2'; Mair & Wilcox 2020) (trimmed level of the mean = 0.1) in the case of individual elements and stable isotopes. These analyses were performed separately for each cohort. In addition, we compared the similarity on the multi-elemental chemical signature of the otolith for all pairs of individuals within each nursery and between pairs of nurseries, by calculating the elemental fingerprinting index (EFI) as described by Moll et al. (2019). The EFI is a measure of similarity between 2 given fish that ranges between 0 and 1, where a value of 0 indicates maximum dissimilarity and 1 indicates highest similarity. Multivariate data were reduced to 2 dimensions and visualized with a canonical analysis of principal coordinates (CAP) using the 'CAPdiscrim' function ('BiodiversityR') (Anderson & Willis 2003, Kindt & Coe 2005).

We then assessed the degree of importance of each element for correctly assigning YOY yellowfin tuna to their nursery area. For that, random forest (RF) classifications were developed (Breiman 2001), which perform best in the presence of skewness (Jones et al. 2017). Data were split into a training dataset (75%) and a testing dataset (25%). We implemented the classification algorithm with the 'randomForest' function (Liaw & Wiener 2002) (number of trees = 500, mtry = 2) and assessed the degree of importance of each element for correctly assigning YOY yellowfin tuna to their nursery area with the 'importance' function ('randomForest'). Variable importance was determined for each element as the mean decrease in accuracy (MDA), when that element was permuted across all trees, and all other elements were left unchanged (Liaw & Wiener 2002). This procedure was randomly repeated 1000 times, and average MDA values for each element were extracted. Elements contributing to a cumulative importance >90% were kept for subsequent classification analyses, which aimed to test the ability of the selected elements to discriminate among nursery areas. After

that, data containing only selected elements were split again into a training dataset (75%) and a testing dataset (25%), and this procedure was randomly repeated 1000 times. At each time, the rate of classification success (i.e. rate of correctly predicted membership to nurseries in which the fish were collected) was calculated, and mean values were extracted. The overall performance of RF to discriminate between groups was also evaluated using the weighted Cohen's Kappa (κ) statistic, a method that accounts for the agreement occurring just by chance (Titus et al. 1984). RF was performed separately for each cohort.

3. RESULTS

3.1. YOY – estimates

The YOY yellowfin tuna used for otolith analyses ranged from 19.5 to 37.5 cm FL, and, according to the age–length relationship calculated in Section 2.2 (Fig. 3), were estimated between 52 and 107 d, or 1.7 and 3.6 mo. Mean hatch dates differed between nurseries and years (Fig. S3). Samples collected in 2018 hatched from November 2017 to May 2018 and were assigned to the 2017 cohort (hereafter '2017').

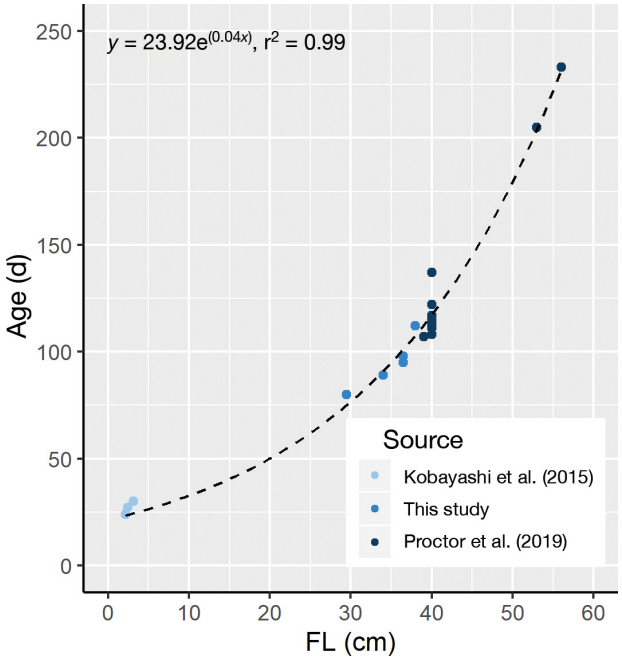

Fig. 3. Age–length (fork length, FL) relationship for young-of-the-year yellowfin tuna *Thunnus albacares* based on *in situ* measures calculated from cultured yellowfin tuna larvae (Kobayashi et al. 2015), and daily age estimates derived from otolith micro-increment counts made by Proctor et al. (2019) and this study

Table 2. Daily increment counts at 65 µm from the primordium and at the inflection point (IP) on otolith transverse sections of 5 young-of-the-year yellowfin tuna *Thunnus albacares* from the West Indian Ocean. Size is fork length (FL) in cm

Individual ID	FL	Days at 65 µm	Days at IP
YFT-001	29.5	12	30
YFT-010	34	11	26
YFT-026	36.5	10	34
YFT-028	36.5	9	31
YFT-036	38	9	28
Mean (SD)	34.9 (3.0)	10.2 (1.3)	29.8 (3.0)

Samples collected in 2019 were hatched from August 2018 to January 2019 were assigned to the 2018 cohort (hereafter '2018'). Mean ± SD age at 65 µm from the primordium was estimated to be 10.2 ± 1.3 d, and to the inflection point was 29.8 ± 3.0 d; these were considered representative of the larval and early juvenile phases, respectively (Table 2).

3.2. Elemental distribution across otoliths

Two-dimensional mapping of trace elements with fs-HR-LA-ICPMS revealed temporal and/or spatial heterogeneity of elemental distributions across otolith sections for the 3 individuals analysed (Fig. 4). In all 3 fish, concentrations of Li were higher during the first month of life, while Sr and Ba concentrations were higher in the otolith portion associated with early larval life stage, with a decrease after ~10 d post hatch. Concentrations of these elements were low around the first month of life, but Sr increased again in the otolith edge of 2 of the individuals analysed, and an increase in concentrations was detected for Ba after fish transitioned into the juvenile stage, increasing thereafter to the otolith edge. Concentrations of Mg and Mn showed distinct distribution patterns on 2 different planes. A gradient of concentration that was perpendicular to the growth axis was evident, from low values on the proximal side of the otolith to larger values on the distal side of the otolith. On the distal side, temporal variations in Mg and Mn were visible. Concentrations of Mg were highest in the otolith portion corresponding to the early larval stage, whereas maximum values of Mn were detected after this period. Concentrations of Cu and Zn were consistently low across the whole section. Overall, high trace element concentrations were detected at the otolith margins (Fig. 4), but in most cases these high values were likely to be an artefact related to a decrease in $CaCO_3$ concentration (Fig. S4).

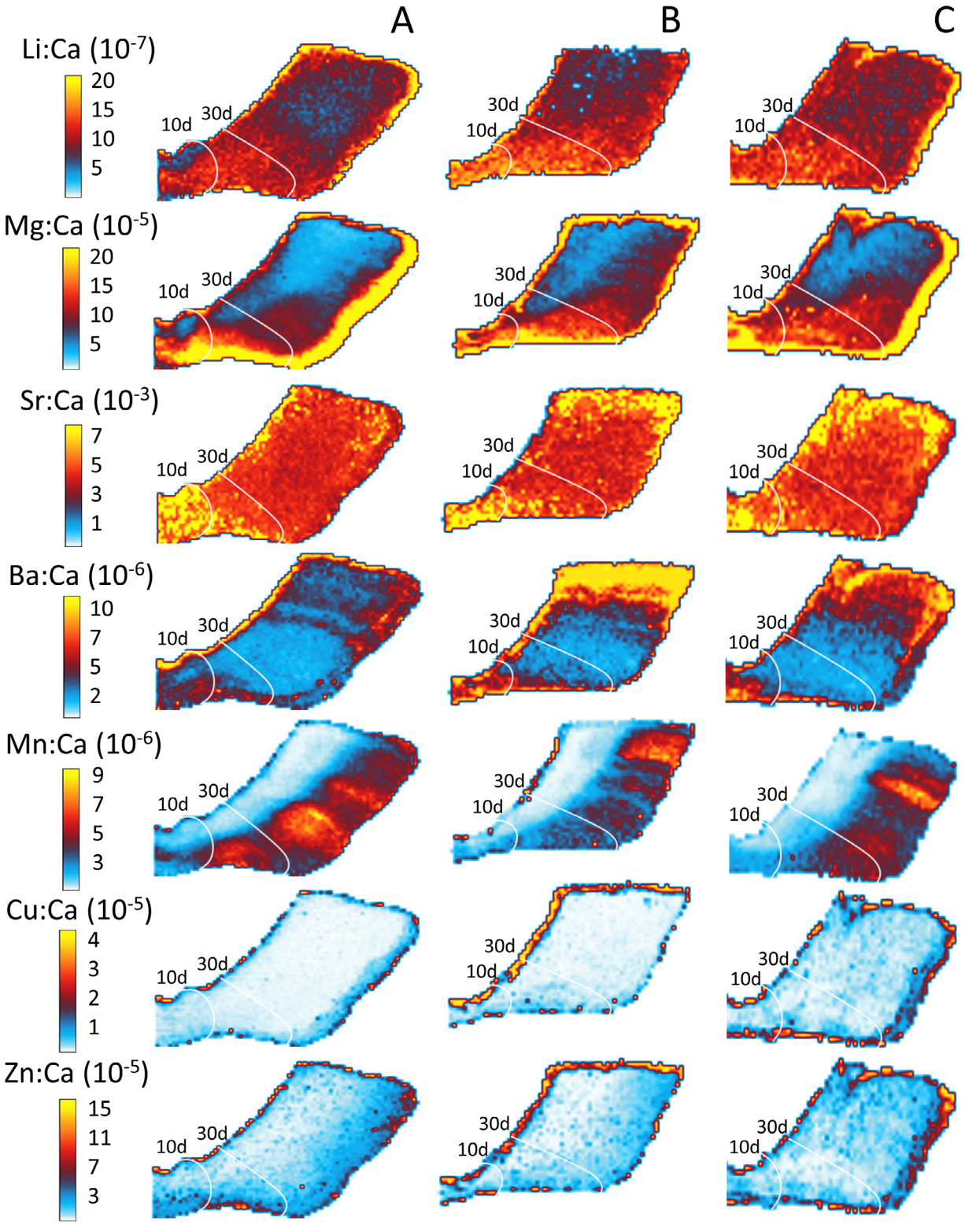

Fig. 4. Trace element 2D maps of ^{7}Li, ^{24}Mg, ^{88}Sr, ^{138}Ba, ^{55}Mn, ^{63}Cu and ^{66}Zn ratios to ^{43}Ca, of 3 young-of-the-year yellowfin tuna *Thunnus albacares* caught in (A) Seychelles-Somalia, (B) Maldives and (C) Sumatra. Fish were collected during May, August and April and with a size of 37, 35 and 32 cm fork length, respectively. Image shows the ventral arm of sagittal otolith transverse sections. Colour indicates element concentration (ppm), ranging from low (white) to high (yellow). Approximate positions of 10 and 30 d growing bands are noted

3.3. Variation in nursery signatures

Significant differences were detected between nurseries and/or cohorts for some of the elements and stable isotopes analysed (PERMANOVA, $p < 0.05$, Table 3). Concentrations of Li varied significantly between cohorts (PERMANOVA, df = 2, p = 0.023, Fig. 5). There were significant differences in Mg and Sr concentrations between nurseries (PERMANOVA, df = 3, p = 0.030 and 0.002, respectively). Concentrations of Mg were higher in Sumatra than in the Maldives, while Sr was higher in the Maldives than in Seychelles-Somalia, but both differences were only significant in 2018 (heteroscedastic 1-way ANOVA post hoc, p = 0.027 and 0.039, respectively). Sr concentrations differed significantly between cohorts (PERMANOVA, df = 1, p = 0.018), with concentrations being higher in 2018 (Fig. 5). No differences in Ba concentrations were detected; concentrations were similar in all nurseries and between cohorts (Fig. 5, Table 3). Concentrations of Mn differed between nurseries (PERMANOVA, df = 3, p = 0.001), but significant interaction between nursery and cohort was also detected (PERMANOVA, df = 2, p = 0.001). In 2017, Mn concentrations were higher in Sumatra than in any other nursery, while in 2018, concentrations were higher in the Maldives than in Seychelles-Somalia (Fig. 5). C and O stable isotope values differed significantly between nurseries (PERMANOVA, df = 3, p = 0.001, and p = 0.001, respectively), with higher values in the western nurseries (Madagascar and Seychelles-Somalia) and decreasing towards the east (Fig. 5). Observed temporal variations were mainly derived by differences in fish belonging to the Maldives nursery, with Li, Mg, Sr and Mn concentrations differing among fish from different cohorts (Table S4).

Table 3. Summary of 2-factor PERMANOVA for the effect of nursery and cohort on individual and combined trace element and stable isotopes of yellowfin tuna *Thunnus albacares* otoliths. Nursery region and cohort were fixed factors within the full factorial design. Significant effects are indicated by asterisks: $^{*}p < 0.05$, $^{**}p < 0.01$

Element	Source	df	*F*	p
Li	Nursery	3	0.87	0.470
	Cohort	1	2.38	0.119
	Nursery × Cohort	2	3.50	0.023*
Mg	Nursery	3	2.79	0.030*
	Cohort	1	0.12	0.730
	Nursery × Cohort	2	1.98	0.141
Sr	Nursery	3	5.20	0.002**
	Cohort	1	5.22	0.018*
	Nursery × Cohort	2	0.95	0.397
Ba	Nursery	3	0.80	0.517
	Cohort	1	0.19	0.686
	Nursery × Cohort	2	1.07	0.358
Mn	Nursery	3	8.27	0.001**
	Cohort	1	0.63	0.418
	Nursery × Cohort	2	10.07	0.001*
$\delta^{13}C$	Nursery	3	11.45	0.001**
	Cohort	1	3.65	0.069
	Nursery × Cohort	2	0.06	0.942
$\delta^{18}O$	Nursery	3	36.76	0.001**
	Cohort	1	0.45	0.495
	Nursery × Cohort	2	1.13	0.336
All	Nursery	3	7.37	0.001**
	Cohort	1	1.83	0.113
	Nursery × Cohort	2	2.62	0.006**

When all individual trace elements and stable isotopes were combined into a single matrix, multielement otolith composition varied significantly between regions (PERMANOVA, df = 3, p = 0.001). The interaction between nursery and cohort was also significant (PERMANOVA, df = 2, p = 0.006). Posterior pairwise comparisons showed that in both cohorts, fish from Seychelles-Somalia, Maldives and Sumatra nurseries were significantly different in their multielemental composition (Table 4). Madagascar, from which only 1 cohort was sampled, was not differentiated from Seychelles-Somalia (pairwise PERMANOVA, p = 0.144), but was different from the Maldives and Sumatra nurseries (Table 4). Multielemental composition of individuals within the same nursery varied mostly in Sumatra, which was also characterised by having the most distinct individuals (lower EFI values) when comparing individual fingerprints between nurseries (Fig. 6). This differentiation of fish from the Sumatra nursery was mainly driven by Mn in 2017 and Mg in 2018 (Fig. 7). Individual fingerprints were more similar among and within fish from Madagascar and Seychelles-Somalia nurseries (Fig. 6), and were mainly differentiated from fish from the other nurseries by their $\delta^{13}C$ and $\delta^{18}O$ values (Fig. 7). Concentrations of Mn and Sr were the main drivers of differentiation of fish from the Maldives in 2018 (Fig. 7).

Due to the absence of difference in the multielemental signature from fish from Madagascar and Seychelles-Somalia nurseries, the latter were combined and treated as a single group, hereafter 'West Indian Ocean', for classification purposes. O was the most important variable in predicting nursery origin based on calculated mean decrease in accuracy score, regardless of the cohort. Mn and Sr were also selected in both classification models (Table 5). High classification success (i.e. ≥80) was observed for sam-

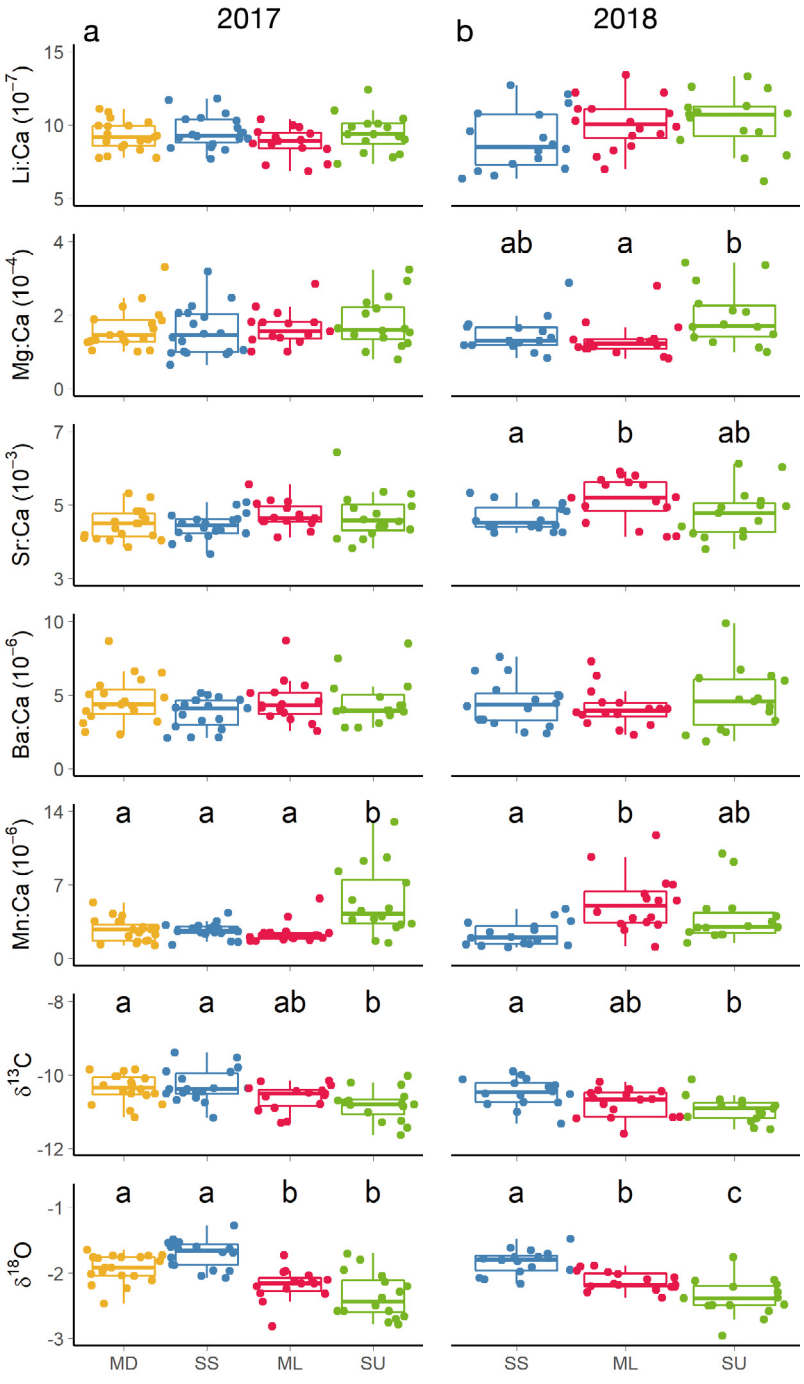

Fig. 5. Regional comparisons of otolith element:Ca ratios and stable isotope (‰) composition for young-of-the-year yellowfin tuna *Thunnus albacares* collected in 4 nursery areas in the Indian Ocean (MD: Madagascar; SS: Seychelles-Somalia; ML: Maldives; SU: Sumatra) for the 2017 and 2018 cohorts. Letters identify significant differences ($p < 0.05$) between regions within a cohort. Interquartile range (25th and 75th percentiles) is shown by extent of boxes, and error bars represent the 10th and 90th percentiles. Median (50th percentile) is also shown. Dots represent individuals

ples from the Western Indian Ocean regardless of the cohort, while nursery-specific classification accuracy was moderate for samples from the Maldives in both cohorts (Table 5). Classification accuracy greatly varied by cohort for YOY from the Sumatra nursery, 58% in 2017 and 70% in 2018. Overall classification success was higher in 2018 (71% and κ = 0.56) than in 2017 (69% and κ = 0.51).

4. DISCUSSION

The aim of this study was to describe chemical signatures in YOY yellowfin tuna otoliths captured in 4 major nursery areas of the Indian Ocean so that they can be used as a baseline to identify the nursery origin of older fish. First, we obtained daily age information on otoliths to provide an approximate scale to assist the interpretation of otolith microchemistry. We then considered the elemental distribution across otolith sections, to better select the elements and the portion of the otolith on which to perform spot analyses. Last, we assessed the potential of chemical signatures to discriminate among different YOY yellowfin tuna nursery areas in the Indian Ocean.

4.1. YOY age estimates

Yellowfin tuna growth-related information has been very limited in the Indian Ocean until the data obtained from the Indian Ocean Tuna Tagging Program became available (Eveson et al. 2015, Sardenne et al. 2015). However, the aim of these studies was to provide relevant information for stock assessment models, and as such small size categories have often been underrepresented. The preliminary age–length curve described in the current study for YOY indicates that yellowfin tuna between 19.5 and 37 cm FL were 52–107 d old. Our results are similar to those obtained for small yellowfin tuna from the western Pacific Ocean (Yamanaka 1990). The portion of the otolith that was 65 µm from the primordium was estimated to represent the signature corresponding to the first ~10 d

Table 4. Summary of pairwise PERMANOVA for multi-elemental signature comparison of yellowfin tuna *Thunnus albacares* otoliths collected in 4 distinct nursery areas. Significant differences are indicated by asterisks: *p < 0.05, **p < 0.01; Signif.: Significance

	F	p	Adjusted p	Signif.
2017				
Madagascar vs. Seychelles-Somalia	1.66	0.144	0.144	
Madagascar vs. Maldives	2.30	0.034	0.041	*
Madagascar vs. Sumatra	5.42	0.001	0.002	**
Seychelles-Somalia vs. Maldives	6.14	0.001	0.002	**
Seychelles-Somalia vs. Sumatra	8.44	0.001	0.002	**
Maldives vs. Sumatra	2.93	0.028	0.041	*
2018				
Seychelles-Somalia vs. Maldives	6.75	0.001	0.002	**
Seychelles-Somalia vs. Sumatra	6.96	0.001	0.002	**
Maldives vs. Sumatra	3.04	0.001	0.011	*

after hatching. Our results are similar those described by Proctor et al. (2019) (i.e. 9 d). The shift from the yolk-sac phase to preflexion larvae is described to occur at 4 d post hatching in yellowfin tuna (Kaji et al. 1999). By placing the spot for microchemical analyses at a location ~10 d from the primordium, we reduced the potential effect of maternal investment (via the yolk sack), which may diminish the ability to delineate natal origins (Ruttenberg et al. 2005, Hegg et al. 2019). The position on the transverse section where a shift in growth direction can be observed (i.e. the inflection point) was estimated to correspond to ~30 d of life of YOY yellowfin tuna. This point represents the metamorphosis from larval to early juvenile, which has also been described to occur around 1 mo after hatching in laboratory-reared yellowfin tuna (Kaji et al. 1999).

4.2. Elemental distribution across otoliths

The use of transversal sections is a well-established practice in tuna otolith microchemistry studies (Macdonald et al. 2013, Fraile et al. 2016, Rooker et al. 2016, Kitchens et al. 2018). However, to our knowledge, elemental distribution patterns throughout these sections in tuna otolith transverse sections had not been described to date. Concentrations of Li, Sr and Ba proved to be relatively homogeneously incorporated within growth increments. These elements are primarily bound into the salt fraction of the otolith, Li likely incorporated by random trapping in interstitial spaces, and Sr and Ba by random replacement of Ca (Doubleday et al. 2014, Izzo et al. 2016, Hüssy et al. 2020). We showed that otolith Li concentrations were higher during the first month of life in all 3 fish, with a decrease thereafter. Otolith growth rates may influence Li incorporation, the latter decreasing with age (Macdonald et al. 2020). Concentrations of Sr and Ba were high during the first 10 d of life, lowest in the adjacent portion and then increased again after the first month of life toward the edge of the otolith. Localized core enrichment of Ba relative to adjacent regions of the otolith has been described (Ruttenberg et al. 2005). Otolith cores have also been recorded to be enriched in Mn (Brophy et al. 2004, Ruttenberg et al. 2005, Limburg et al. 2011), and as such this element has been used

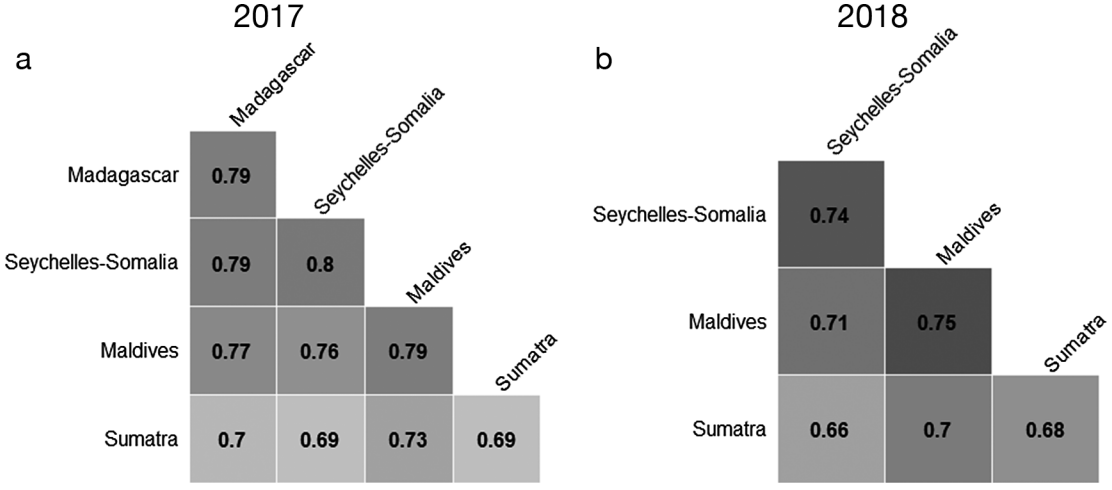

Fig. 6. Mean values of elemental fingerprinting indices (EFI) calculated within each nursery and among nurseries for the 2017 and 2018 cohorts. The EFI ranges from 0 to 1, where a value of 0 indicates that 2 compared individuals are most different in otolith elemental composition, whereas a value of 1 indicates the highest similarity in elemental composition between 2 individuals

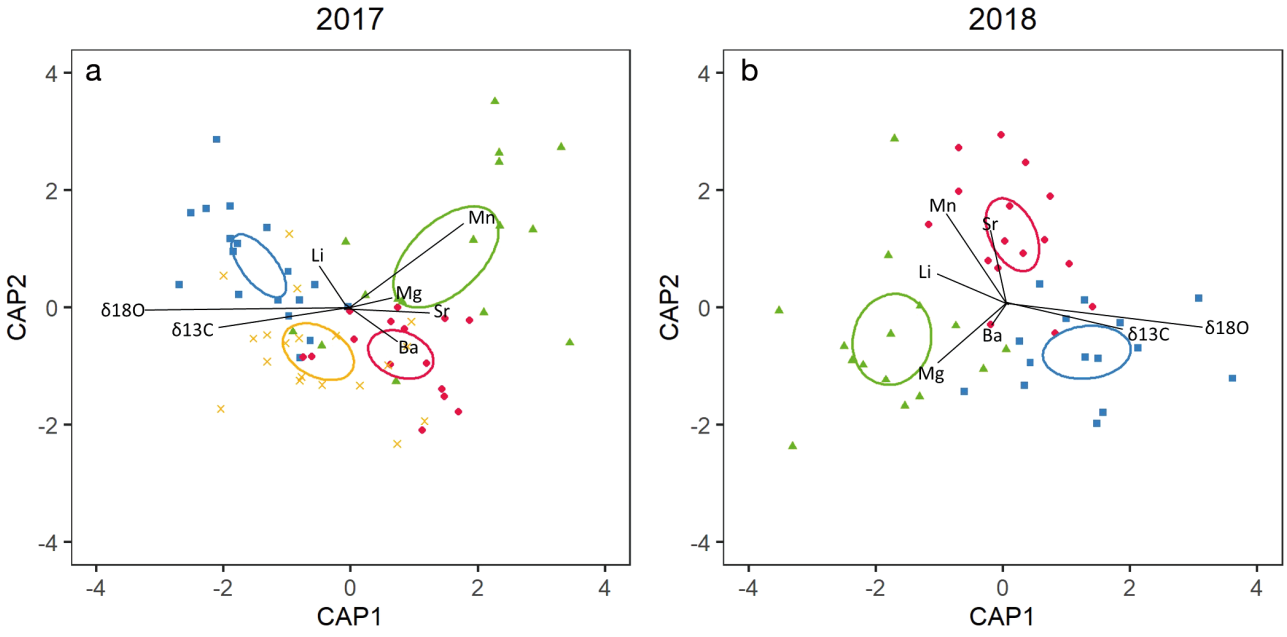

Fig. 7. Canonical analysis of principal coordinates (CAP, constrained ordination) plots showing multi-elemental (Li, Mg, Sr, Ba, Mn, $\delta^{13}C$ and $\delta^{18}O$) chemistry composition of young-of-the-year yellowfin tuna *Thunnus albacares* otoliths from 4 nursey areas in the Indian Ocean (Madagascar: yellow crosses; Seychelles-Somalia: blue squares; Maldives: red circles; Sumatra: green triangles) for the 2017 and 2018 cohorts. Ellipses represent 95% confidence limits around each multivariate mean, and biplot vectors show the relative influence of each element to nursery discrimination

as a marker for otolith primordium detection (Macdonald et al. 2008, Rogers et al. 2019). However, we did not observe this pattern in any of the 3 YOY yellowfin tuna Mn distribution maps, but the maximum values of Mn were shown in parts of the otolith other than the core. Most of the otolith microchemistry studies that describe otolith core Mn enrichment, however, belong to benthic or demersal fish species with very different life strategies compared to yellowfin tuna. Indeed, studies on tuna species show elevated Mn concentrations not just in the primordium, but some weeks after (Wang et al. 2009, Macdonald et al. 2013, Artetxe-Arrate et al. 2019).

Table 5. Random forest classification success in assigning young-of-the-year yellowfin tuna *Thunnus albacares* collected in the Indian Ocean to their nursery of origin based on otolith chemical composition. Results are shown for each sampling cohort. The element combination that resulted in a mean decrease in accuracy cumulative value >90%, by order of importance, is shown. Data represent the percentage (%) of correctly assigned individuals to their nursery area; West Indian Ocean (Madagascar + Seychelles-Somalia), Maldives and Sumatra. Overall accuracy and kappa index (κ) are also shown

Cohort	Element combination	West Indian Ocean	Maldives	Sumatra	Overall	κ
2017	$\delta^{18}O$, Mn:Ca, Sr:Ca	80	55	58	69	0.51
2018	$\delta^{18}O$, Mn:Ca, Mg:Ca, Sr:Ca	80	62	70	71	0.56

The distribution of Mg and Mn in the otolith showed a gradient of concentration within the growth bands, with lower concentrations closer to the proximal side of the transverse section. Otolith chemical heterogeneity has also been described in other species, although the ultimate cause of these variations is still unknown (Di Franco et al. 2014, Limburg & Elfman 2017). Both Mg and Mn are important co-factors required for the enzymatic activity involved in the biomineralization process and, as such, influenced by physiological control on uptake mechanisms and can be incorporated into the proteinaceous fraction of the otolith (Loewen et al. 2016, Thomas & Swearer 2019, Hüssy et al. 2020). It has been suggested that the preferential binding of the elements into either the protein or mineral component can result in heterogeneous distribution of elements throughout the otolith structure (Izzo et al. 2016). Finally, Cu and Zn concentrations were generally low within the whole otolith section. Elsdon et al. (2008) described that Cu and Zn may leach out from the otolith during storage. Moreover, these elements are bound to soluble otolith proteins, and are important co-factors in many enzymes (Miller et al. 2006, Hüssy et al. 2020). Thus, the inclusion of these

elements into natal delineation studies may add noise and obscure spatial variation in chemical signatures (Thomas et al. 2020). Given this, Cu and Zn were discarded for posterior analyses aiming to describe the natal signatures of YOY yellowfin tuna from the Indian Ocean.

Following recent progress in instrumentation and mapping software, 2-dimensional spatial images of elemental distributions are increasingly being used to provide valuable visualizations of chemical heterogeneity across the otolith (McGowan et al. 2014, Walther 2019). The observed variations in YOY yellowfin tuna otolith sections may be useful to select the portion of otoliths for spot ablations or transect analyses that maximizes discrimination among groups, at the same time as minimizing the noise introduced by the intrinsic factors of individual fish.

4.3. Variation in nursery signatures

Regional differences in otolith chemistry were detected for YOY yellowfin tuna collected from 4 nursery areas in the Indian Ocean. The multi-elemental chemical signatures of YOY yellowfin tuna from Seychelles-Somalia, Maldives and Sumatra were significantly different for both cohorts analysed, while fish from Madagascar were not differentiated from those from Seychelles-Somalia, contrary to what was shown in a previous study (Artetxe-Arrate et al. 2019). In that study, however, YOY yellowfin tuna from both nursery areas were from different cohorts, and results from the present study highlight that the cohort effect may strongly influence otolith trace element data composition. In any case, the absence of difference does not necessarily imply that fish shared a common origin, but that the technique is of negligible value to discriminate among these 2 nurseries at this time (Campana et al. 2000). Likewise, the variability in the chemical signature within individuals from Sumatra was almost as high as the difference with samples from any other nursery. It is possible that factors other than ambient water chemistry, such as metabolic sources, variation in genotype, growth rates and/or physiological processes, have influenced the observed among-individual variability in fish from the Sumatra nursery (Macdonald et al. 2008, Clarke et al. 2011, Sturrock et al. 2015). Indeed, high Mn and Mg concentrations were the main drivers of differentiation of YOY yellowfin tuna from the Sumatra nursery for the 2017 and 2018 cohorts, respectively. Uptake mechanisms for these elements into the otoliths are under considerable physiological control (Hüssy et al. 2020). High concentrations of Mn were also detected for 2018 cohort YOY from the Maldives relative to other nurseries. Mn availability increases in the presence of hypoxia and other redox environments (Limburg & Casini 2018), and therefore otolith Mn concentrations have been identified as a potentially reliable proxy of fish exposure to hypoxia (Limburg et al. 2011, 2015). Nevertheless, it is unlikely that differences in exposure to hypoxia are driving the observed Mn pattern in YOY yellowfin tuna from different nurseries. We specifically sampled otoliths at a life stage corresponding to the first 10 d of life, when yellowfin tuna are still at a preflexion larval stage and inhabit the first 20 m of the water column, where low oxygen levels do not normally occur (Boehlert & Mundy 1994, Kaji et al. 1999, Wexler et al. 2011). Thus, we concluded that observed differences in Mn concentrations between nurseries in each year may relate to physiological processes that occurred during biomineralization of the otolith (Hüssy et al. 2020). Increased Sr concentrations were also detected in the 2018 cohort of YOY yellowfin tuna from the Maldives. Sr is a trace element that is positively related to its ambient concentration, and the interaction between temperature and salinity affects otolith Sr concentrations (Bath et al. 2000, Elsdon & Gillanders 2002, Walther & Thorrold 2006). The area west of the Maldives is characterised by having an annual cycle and ecological regime distinct from the surrounding regions, with a strong zonal advection (Huot et al. 2019, Bao et al. 2020). These environmental peculiarities of the Maldives may have led to the observed differences in otolith Sr concentrations with respect to the Seychelles-Somalia nursery.

C and O stable isotopes were an important source of differentiation between nurseries. Otolith $\delta^{13}C$ has been recently described as a proxy for metabolic rate in fish (Chung et al. 2019). Otolith $\delta^{13}C$ is influenced by the environment (dissolved inorganic carbon in water) and diet, and significantly affected by temperature (Martino et al. 2019). The observed carbon isotope trend in YOY yellowfin tuna otoliths, decreasing west to east, followed the expected trend according to Indian Ocean water temperature distribution (Fingas 2019). Ambient temperature is also an accurate proxy of otolith $\delta^{18}O$ (Macdonald et al. 2020). Although other intrinsic factors, such as growth and physiology, may influence otolith $\delta^{18}O$ incorporation, variations in otolith $\delta^{18}O$ closely reflect the ambient temperature experienced by the fish, being inversely correlated with ambient seawater temperature (Kitagawa et al. 2013, Darnaude & Hunter 2018, Macdon-

ald et al. 2020). Otolith oxygen isotope ratios of YOY yellowfin tuna from the Indian Ocean followed the expected trend (Fig. S5), presenting higher values in the western nurseries (expected lower water temperatures, under the influence of the seasonal Somali upwelling) and decreasing towards the east (expected higher water temperatures, from the Indonesian throughflow) (Schott et al. 2002).

Temporal differences were also evident within nursery chemical composition, particularly in the Maldives nursery. The Indian Ocean is characterised by a seasonal reversal of surface winds, with 2 seasons of distinct wind regimes (i.e. monsoons) that strongly influence the oceanography north of 10° S (Ramage 1969, Schott & McCreary 2001). Due to sampling constraints, 2017 cohort individuals from the Maldives were hatched at the beginning of the boreal summer monsoon, whereas individuals from the 2018 cohort were hatched at the beginning of the boreal winter monsoon. The observed among-cohort differences within YOY yellowfin tuna from the Maldives nursery are probably derived from the physical and biological variations of the region between the 2 monsoonal seasons (Huot et al. 2019). Interannual differences in trace element data may also be due to the fact that these signatures represented a very short time frame of the early life of the fish (i.e. days), contrary to stable isotope data, which represent a longer time frame (i.e. months). As such, trace element data did not represent an average of regional scale oceanographic conditions, but particular conditions at the given period. However, by increasing the time frame analysed for trace element analyses, the obtained signal could have reflected a mixture of extrinsic and intrinsic (e.g. ontogenetic) influences that may have increased individual variability in otolith chemistry (Macdonald et al. 2020, Thomas et al. 2020).

A substantial proportion of YOY yellowfin tuna (69–71%) were correctly assigned to their origin when analysed separately for each cohort, but nursery-specific classification success was higher in 2018 for Maldives and Sumatra. Interannual differences in region-specific classification have also been reported in other yellowfin tuna nurseries of the Atlantic and Pacific Oceans based on otolith microchemistry (Wells et al. 2012, Rooker et al. 2016, Kitchens et al. 2018), which highlights the importance of constructing year-by-year reference baseline signatures. The inclusion of trace element data to the baseline of $\delta^{13}C$ and $\delta^{18}O$ stable isotope signatures did not significantly improve classification success in yellowfin tuna from the Pacific Ocean nurseries (Rooker et al. 2016), while trace elements proved to be more effective to discriminate among yellowfin tuna nurseries in the Atlantic Ocean (Kitchens et al. 2018). Here, the most important predictor signatures for models tested included $\delta^{18}O$ and Mn:Ca and Sr:Ca ratios. O values were the main driver of differentiation between nurseries in the west (Madagascar and Seychelles-Somalia), and those in the central–east (Maldives and Sumatra), but the addition of trace elements allowed for finer-scale nursery discrimination. Thus, the effort to incorporate trace element ratios into otolith chemistry baselines for yellowfin tuna in the Indian Ocean may benefit from higher power of discrimination but will require age-class matching when adults are assigned to these combined baseline of nursery signatures.

4.4. Conclusions and future directions

Described age estimates provided an accurate temporal scale to assist the interpretation of otolith microchemistry of YOY yellowfin tuna data and to link assay locations with early life history stages. Two-dimensional visualization was useful to gain insights of elemental distribution patterns. The present study shows that some elements exhibit a disjunct accumulation in yellowfin tuna otoliths (i.e. difference in elemental concentration among parts of an otolith corresponding to the same fish age). This is an important issue to consider when, for example, selecting elemental assay locations. Arbitrarily laid transects or spots can differ in element composition among samples just because of their placement. Thus, we strongly recommend sampling the same otolith axis within (and ideally across) studies to avoid misinterpretations of the results and/or to investigate the homogeneity of element composition within the otolith prior to any otolith microchemistry study. As the elemental signatures of YOY yellowfin tuna varied among nurseries, the baseline signature described in this study may be used as an effective tool to assign juvenile and adult individuals to their nursery origin. However, temporal variability of trace element concentrations is an important aspect to be considered, and future classifications of older individuals to nursery areas will require that the individuals being characterised belong to the same year classes as the baseline used as a reference. These cohort-matched reference baselines will provide insights into the connectivity and mixing rates of older individuals within the Indian Ocean, as well as the contribution of each nursery area to the overall population. This information will have important implications for

fisheries management, as the understanding of stock structure helps determine the appropriate unit for stock assessment and suitable spatial scales for management.

Acknowledgements. We thank Campbell Davies, Francis Marsac and Zulkarnaen Fahmi, who planned and coordinated the sampling design and were responsible together with Hilario Murua for the PSTBS-IO project to go forward. We also thank the many people who were involved in the collection of the otoliths used for this study: Iñigo Krug, Natacha Nikolic, Anais Médieu, Mohamed Ahusan, Matt Landsdell, Craig Proctor, Asep Priatna, Pratiwi Lestari, Achmad Zamroni and Muhammad Taufik; we are grateful for all of their efforts. We thank the many vessel owners, skippers, observers, crews and processors who provided fish for sampling, and the Seychelles Fishing Authority for facilitating access to sample processing in the Seychelles. Thanks also to Gaelle Barbotin for her technical assistance in trace element analyses and to Isabel Garcia-Baron and Igor Granado for their help with the coding. Funding for this work was provide by the European Union (Grant number S12.697993) and the FAO/IOTC, within the framework of a collaborative project (GCP/INT/233/EC – Population structure of IOTC species in the Indian Ocean) between FAO/IOTC and CSIRO Oceans and Atmosphere, AZTI, Institut de Recherche pour le Développement (IRD) and Indonesia's Center for Fisheries Research (CFR). The views expressed herein can in no way be taken to reflect the official opinion of the European Union. I.A.A. was funded by a PhD research grant from the Department of Agriculture, Fisheries and Food Policy from the Basque Government (Convocatoria ayudas de formación a jóvenes investigadores y tecnólogos 2017). This document is contribution no. 1066 from AZTI, Marine Research, Basque Research and Technology Alliance (BRTA).

LITERATURE CITED

Anderson MJ (2001) A new method for non-parametric multivariate analysis of variance. Austral Ecol 26:32–46

Anderson M, Willis T (2003) Canonical analysis of principal coordinates: a useful method of constrained ordination for ecology. Ecology 84:511–525

Artetxe-Arrate I, Fraile I, Crook D, Zudaire I, Arrizabalaga H, Greig A, Murua H (2019) Otolith microchemistry: a useful tool for investigating stock structure of yellowfin tuna (*Thunnus albacares*) in the Indian Ocean. Mar Freshw Res 70:1708–1721

Bao S, Wang H, Zhang R, Yan H, Chen J (2020) Spatial and temporal scales of sea surface salinity in the tropical Indian Ocean from SMOS, Aquarius and SMAP. J Oceanogr 76: 389–400

Bath G, Thorrold S, Jones C, Campana S (2000) Strontium and barium uptake in aragonitic otoliths of marine fish. Geochim Cosmochim Acta 64:1705–1714

Benjamini Y, Hochberg Y (1995) Controlling the false discovery rate: a practical and powerful approach to multiple testing. J R Stat Soc B 57:289–300

Boehlert GW, Mundy BC (1994) Vertical and onshore–offshore distributional patterns of tuna larvae in relation to physical habitat features. Mar Ecol Prog Ser 107:1–13

Bosley KM, Goethel DR, Berger AM, Deroba JJ and others (2019) Overcoming challenges of harvest quota allocation in spatially structured populations. Fish Res 220:105344

Breiman L (2001) Random forests. Mach Learn 45:5–32

Brophy D, Jeffries TE, Danilowicz BS (2004) Elevated manganese concentrations at the cores of clupeid otoliths: possible environmental, physiological, or structural origins. Mar Biol 144:779–786

Campana SE (1999) Chemistry and composition of fish otoliths: pathways, mechanisms and applications. Mar Ecol Prog Ser 188:263–297

Campana SE, Neilson JD (1985) Microstructure of fish otoliths. Can J Fish Aquat Sci 42:1014–1032

Campana SE, Thorrold SR (2001) Otoliths, increments, and elements: keys to a comprehensive understanding of fish populations? Can J Fish Aquat Sci 58:30–38

Campana SE, Chouinard GA, Hanson JM, Fréchet A, Brattey J (2000) Otolith elemental fingerprints as biological tracers of fish stocks. Fish Res 46:343–357

Chung M, Trueman C, Godiksen J, Grønkjær P (2019) Otolith $\delta^{13}C$ values as a metabolic proxy: approaches and mechanical underpinnings. Mar Freshw Res 70:1747–1756

Clarke LM, Thorrold SR, Conover DO (2011) Population differences in otolith chemistry have a genetic basis in *Menidia menidia*. Can J Fish Aquat Sci 68:105–114

Claverie F, Fernández B, Pécheyran C, Alexis J, Donard OFX (2009) Elemental fractionation effects in high repetition rate IR femtosecond laser ablation ICP-MS analysis of glasses. J Anal At Spectrom 24:891–902

Conand F, Richards WJ (1982) Distribution of tuna larvae between Madagascar and the Equator, Indian Ocean. Biol Oceanogr 1:321–336

Dammannagoda S, Hurwood D, Mather P (2008) Evidence for fine geographical scale heterogeneity in gene frequencies in yellowfin tuna (*Thunnus albacares*) from the north Indian Ocean around Sri Lanka. Fish Res 90: 147–157

Darnaude AM, Hunter E (2018) Validation of otolith $\delta^{18}O$ values as effective natural tags for shelf-scale geolocation of migrating fish. Mar Ecol Prog Ser 598:167–185

Davies C, Marsac F, Murua H, Fraile I and others (2020) Study of population structure of IOTC species and sharks of interest in the Indian Ocean using genetics and microchemistry: 2020 Final Report to IOTC. CSIRO

Di Franco A, Bulleri F, Pennetta A, De Benedetto G, Clarke KR, Guidetti P (2014) Within-otolith variability in chemical fingerprints: implications for sampling designs and possible environmental interpretation. PLOS ONE 9: e101701

Doubleday ZA, Harris HH, Izzo C, Gillanders BM (2014) Strontium randomly substituting for calcium in fish otolith aragonite. Anal Chem 86:865–869

Elsdon TS, Gillanders BM (2002) Interactive effects of temperature and salinity on otolith chemistry: challenges for determining environmental histories of fish. Can J Fish Aquat Sci 59:1796–1808

Elsdon TS, Wells BK, Campana SE, Gillanders BM, Jones CM, Limburg KE, Walther BD (2008) Otolith chemistry to describe movements and life-history parameters of fishes: hypotheses, assumptions, limitations and inferences. Oceanogr Mar Biol Annu Rev 46:297–330

Eveson J, Million J, Sardenne F, Croizier GL (2015) Estimating growth of tropical tunas in the Indian Ocean using tag-recapture data and otolith-based age estimates. Fish Res 163:58–68

FAO (2016) The state of world fisheries and aquaculture 2016. Contributing to food security and nutrition for all. FAO, Rome

FAO (2020) Fishery statistical collections. www.fao.org/fishery/statistics/global-capture-production/query/en (accessed 1 April 2020)

Fingas M (2019) Remote sensing for marine management. In: Sheppard C (ed) World seas: an environmental evaluation, 2nd edn. Academic Press, Cambridge, MA, p 103–119

Fraile I, Arrizabalaga H, Santiago J, Goñi N and others (2016) Otolith chemistry as an indicator of movements of albacore (*Thunnus alalunga*) in the North Atlantic Ocean. Mar Freshw Res 67:1002–1013

Guillotreau P, Squires D, Sun J, Compeán GA (2017) Local, regional and global markets: What drives the tuna fisheries? Rev Fish Biol Fish 27:909–929

Hegg JC, Kennedy BP, Chittaro P (2019) What did you say about my mother? The complexities of maternally derived chemical signatures in otoliths. Can J Fish Aquat Sci 76: 81–94

Huot Y, Antoine D, Daudon C (2019) Partitioning the Indian Ocean based on surface fields of physical and biological properties. Deep-Sea Res II 166:75–89

Hüssy K, Limburg KE, de Pontual H, Thomas ORB and others (2020) Trace element patterns in otoliths: the role of biomineralization. Rev Fish Sci Aquacult, https://doi.org/10.1080/23308249.2020.1760204

IOTC (Indian Ocean Tuna Commission) (2020) Status of the Indian Ocean yellowfin tuna (YFT: *Thunnus albacares*) resource. Executive summary. www.iotc.org/sites/default/files/Yellowfin2020.pdf (accessed 3 December 2020)

IOTC (2021) Yellowfin tuna supporting information. www.iotc.org/sites/default/files/content/Stock_status/YFT_supporting_information_July2021.pdf (accessed 17 August 2021)

ISSF (International Seafood Sustainability Foundation) (2020) Status of the world fisheries for tuna. Mar. 2020. Tech Rep 2020-12. ISSF, Washington, DC

Izzo C, Doubleday Z, Gillanders B (2016) Where do elements bind within the otoliths of fish? Mar Freshw Res 67:1072–1076

Jones CM, Palmer M, Schaffler JJ (2017) Beyond Zar: the use and abuse of classification statistics for otolith chemistry. J Fish Biol 90:492–504

Kaji T, Tanaka M, Oka M, Takeuchi H, Ohsumi S, Teruya K, Hirokawa J (1999) Growth and morphological development of laboratory-reared yellowfin tuna *Thunnus albacares* larvae and early juveniles, with special emphasis on the digestive system. Fish Sci 65:700–707

Kerr L, Hintzen N, Cadrin S (2017) Lessons learned from practical approaches to reconcile mismatches between biological population structure and stock units of marine fish. ICES J Mar Sci 74:1708–1722

Kerr L, Whitener Z, Cadrin S, Morse M, Secor D, Golet W (2020) Mixed stock origin of Atlantic bluefin tuna in the US rod and reel fishery (Gulf of Maine) and implications for fisheries management. Fish Res 224:105461

Kindt R, Coe R (2005) Tree diversity analysis. A manual and software for common statistical methods for ecological and biodiversity studies. World Agroforestry Centre (ICRAF), Nairobi

Kitagawa T, Ishimura T, Uozato R, Shirai K and others (2013) Otolith $\delta^{18}O$ of Pacific bluefin tuna *Thunnus orientalis* as an indicator of ambient water temperature. Mar Ecol Prog Ser 481:199–209

Kitchens LL, Rooker JR, Reynal L, Falterman BJ, Saillant E, Murua H (2018) Discriminating among yellowfin tuna *Thunnus albacares* nursery areas in the Atlantic Ocean using otolith chemistry. Mar Ecol Prog Ser 603:201–213

Kobayashi T, Honryo T, Agawa Y, Sawada Y and others (2015) Gonadogenesis and slow proliferation of germ cells in juveniles of cultured yellowfin tuna, *Thunnus albacares*. Reprod Biol 15:106–112

Kunal S, Kumar G, Menezes M, Meena R (2013) Mitochondrial DNA analysis reveals three stocks of yellowfin tuna *Thunnus albacares* (Bonnaterre, 1788) in Indian waters. Conserv Genet 14:205–213

Liaw A, Wiener M (2002) Classification and regression by randomForest. R News 2:18–22

Limburg KE, Casini M (2018) Effect of marine hypoxia on Baltic Sea cod *Gadus morhua*: evidence from otolith chemical proxies. Front Mar Sci 5:482

Limburg KE, Elfman M (2017) Insights from two-dimensional mapping of otolith chemistry. J Fish Biol 90:480–491

Limburg KE, Olson C, Walther Y, Dale D, Slomp CP, Høie H (2011) Tracking Baltic hypoxia and cod migration over millennia with natural tags. Proc Natl Acad Sci USA 108: E177–E182

Limburg KE, Walther BD, Lu Z, Jackman G and others (2015) In search of the dead zone: use of otoliths for tracking fish exposure to hypoxia. J Mar Syst 141:167–178

Loewen TN, Carriere B, Reist JD, Halden NM, Anderson WG (2016) Linking physiology and biomineralization processes to ecological inferences on the life history of fishes. Comp Biochem Physiol A Mol Integr Physiol 202: 123–140

Macdonald JI, Shelley JMG, Crook DA (2008) A method for improving the estimation of natal chemical signatures in otoliths. Trans Am Fish Soc 137:1674–1682

Macdonald JI, Farley JH, Clear NP, Williams AJ, Carter TI, Davies CR, Nicol SJ (2013) Insights into mixing and movement of South Pacific albacore *Thunnus alalunga* derived from trace elements in otoliths. Fish Res 148: 56–63

Macdonald JI, Drysdale RN, Witt R, Cságoly Z, Marteinsdóttir G (2020) Isolating the influence of ontogeny helps predict island-wide variability in fish otolith chemistry. Rev Fish Biol Fish 30:173–202

Mair P, Wilcox RR (2020) Robust statistical methods in R using the WRS2 package. Behav Res Methods 52:464–488

Martinez Arbizu P (2020) pairwiseAdonis: Pairwise multilevel comparison using Adonis. R package version 0.4. https://github.com/pmartinezarbizu/pairwiseAdonis

Martino JC, Doubleday ZA, Gillanders BM (2019) Metabolic effects on carbon isotope biomarkers in fish. Ecol Indic 97:10–16

McGowan N, Fowler AM, Parkinson K, Bishop DP and others (2014) Beyond the transect: an alternative microchemical imaging method for fine scale analysis of trace elements in fish otoliths during early life. Sci Total Environ 494–495:177–186

Miller MB, Clough AM, Batson JN, Vachet RW (2006) Transition metal binding to cod otolith proteins. J Exp Mar Biol Ecol 329:135–143

Moll D, Kotterba P, Jochum KP, von Nordheim L, Polte P (2019) Elemental inventory in fish otoliths reflects natal origin of Atlantic herring (*Clupea harengus*) from Baltic Sea juvenile areas. Front Mar Sci 6:191

Moore B, Lestari P, Cutmore S, Proctor C, Lester R (2019) Movement of juvenile tuna deduced from parasite data. ICES J Mar Sci 76:1678–1689

Muhling BA, Lamkin JT, Alemany F, García A and others

(2017) Reproduction and larval biology in tunas, and the importance of restricted area spawning grounds. Rev Fish Biol Fish 27:697–732

Nishikawa Y, Honma M, Ueyanagi S, Kikawa S (1985) Average distribution of larvae of oceanic species of scombrid fishes, 1956–1981. Far Seas Fish Res Lab S Ser 12:1–99

Nootmorn P, Yakoh A, Kawises K (2005) Reproductive biology of yellowfin tuna in the Eastern Indian Ocean. IOTC-2005-WPTT-14

Oksanen J, Blanchet FG, Friendly M, Kindt R and others (2017) Vegan: community ecology package. R package version 2.4-3. https://CRAN.R-project.org/package=vegan

Pecoraro C, Babbucci M, Franch R, Rico C and others (2018) The population genomics of yellowfin tuna (*Thunnus albacares*) at global geographic scale challenges current stock delineation. Sci Rep 8:13890

Proctor CH, Lester RJG, Clear NP, Grewe PM and others (2019) Population structure of yellowfin tuna (*Thunnus albacares*) and bigeye tuna (*T. obesus*) in the Indonesian region. Final Report. ACIAR Project FIS/2009/059. Australian Centre for International Agricultural Research, Canberra. www.aciar.gov.au/sites/default/files/project-page-docs/fis-2009-059_popstructurestudy_final_report.pdf

R Core Team (2019) R: a language and environment for statistical computing. R Foundation for Statistical Computing, Vienna

Ramage CS (1969) Indian Ocean surface meteorology. Oceanogr Mar Biol Annu Rev 7:11–33

Reglero P, Tittensor DP, Álvarez-Berastegui D, Aparicio-González A, Worm B (2014) Worldwide distributions of tuna larvae: revisiting hypotheses on environmental requirements for spawning habitats. Mar Ecol Prog Ser 501:207–224

Rogers TA, Fowler AJ, Steer MA, Gillanders BM (2019) Discriminating natal source populations of a temperate marine fish using larval otolith chemistry. Front Mar Sci 6: 711

Rooker JR, Wells RJD, Itano DG, Thorrold SR, Lee JM (2016) Natal origin and population connectivity of bigeye and yellowfin tuna in the Pacific Ocean. Fish Oceanogr 25: 277–291

Ruttenberg BI, Hamilton SL, Hickford MJH, Paradis GL and others (2005) Elevated levels of trace elements in cores of otoliths and their potential for use as natural tags. Mar Ecol Prog Ser 297:273–281

Sardenne F, Dortel E, Le Croizier G, Million J and others (2015) Determining the age of tropical tunas in the Indian Ocean from otolith microstructures. Fish Res 163: 44–57

Schaefer KM (2001) Reproductive biology of tunas. In: Block BA, Stevens E (eds) Tuna: physiology, ecology and evolution. Academic Press, San Diego, CA, p 225–270

Schott F, McCreary J (2001) The monsoon circulation of the Indian Ocean. Prog Oceanogr 51:1–123

Schott F, Dengler M, Schoenefeldt R (2002) The shallow overturning circulation of the Indian Ocean. Prog Oceanogr 53:57–103

Sharp GD (2001) Tuna oceanography – an applied science. In: Block B, Stevens G (eds) Tuna: physiology, ecology, and evolution. Academic Press, San Diego, CA, p 345–388

Sturgeon RE, Willie SN, Yang L, Greenberg R and others (2005) Certification of a fish otolith reference material in support of quality assurance for trace element analysis. J Anal At Spectrom 20:1067–1071

Sturrock AM, Hunter E, Milton JA, Johnson RC, Waring CP, Trueman CN (2015) Quantifying physiological influences on otolith microchemistry. Methods Ecol Evol 6: 806–816

Thomas O, Swearer S (2019) Otolith biochemistry — a review. Rev Fish Sci Aquacult 27:458–489

Thomas ORB, Ganio K, Roberts BR, Swearer SE (2017) Trace element–protein interactions in endolymph from the inner ear of fish: implications for environmental reconstructions using fish otolith chemistry. Metallomics 9: 239–249

Thomas ORB, Thomas KV, Jenkins GP, Swearer SE (2020) Spatio-temporal resolution of spawning and larval nursery habitats using otolith microchemistry is element dependent. Mar Ecol Prog Ser 636:169–187

Thorrold S, Campana S, Jones C (1997) Factors determining $\delta^{13}C$ and $\delta^{18}O$ fractionation in aragonitic otoliths of marine fish. Geochim Cosmochim Acta 61:2909–2919

Titus K, Mosher JA, Williams BK (1984) Chance-corrected classification for use in discriminant analysis: ecological applications. Am Midl Nat 111:1–7

Ueyanagi S (1969) Observations on the distribution of tuna larvae in the Indo-Pacific Ocean with emphasis on the delineation of the spawning areas of albacore, *Thunnus alalunga*. Bull Far Seas Fish Res Lab 2:177–256

Walther BD (2019) The art of otolith chemistry: interpreting patterns by integrating perspectives. Mar Freshw Res 70: 1643–1658

Walther BD, Thorrold SR (2006) Water, not food, contributes the majority of strontium and barium deposited in the otoliths of a marine fish. Mar Ecol Prog Ser 311:125–130

Wang CH, Lin YT, Shiao JC, You CF, Tzeng WN (2009) Spatio-temporal variation in the elemental compositions of otoliths of southern bluefin tuna *Thunnus maccoyii* in the Indian Ocean and its ecological implication. J Fish Biol 75:1173–1193

Wells RJD, Rooker JR, Itano DG (2012) Nursery origin of yellowfin tuna in the Hawaiian Islands. Mar Ecol Prog Ser 461:187–196

Wexler JB, Margulies D, Scholey VP (2011) Temperature and dissolved oxygen requirements for survival of yellowfin tuna, *Thunnus albacares*, larvae. J Exp Mar Biol Ecol 404:63–72

Yamanaka KL (1990) Age, growth and spawning of yellowfin tuna in the southern Philippines. PhD dissertation, University of British Columbia, Vancouver

Ying Y, Chen Y, Lin L, Gao T (2011) Risks of ignoring fish population spatial structure in fisheries management. Can J Fish Aquat Sci 68:2101–2120

Zhu G, Xu L, Zhou Y, Song L (2008) Reproductive biology of yellowfin tuna *T. albacares* in the west-central Indian Ocean. J Ocean Univ China 7:327–332

Zudaire I, Murua H, Grande M, Bodin N (2013) Reproductive potential of yellowfin tuna (*Thunnus albacares*) in the western Indian Ocean. Fish Bull 111:252–264

Editorial responsibility: Stephen Wing, Dunedin, New Zealand
Reviewed by: N. Burns, J. Mohan and 1 anonymous referee

Submitted: January 8, 2021
Accepted: May 25, 2021
Proofs received from author(s): August 17, 2021